Characterization of Zirconium Phosphate/Polycation Thin Films Grown by Sequential Adsorption Reactions

Hyuk-Nyun Kim, Steven W. Keller,† and Thomas E. Mallouk*

Department of Chemistry, Pennsylvania State University, University Park, Pennsylvania 16802

Johannes Schmitt

Institut für Physikalische Chemie, Johannes Gutenberg-Universität, D-55099 Mainz, Germany

Gero Decher

Institut Charles Sadron, Université Louis Pasteur, F-67083 Strasbourg Cedex, France

Received January 6, 1997. Revised Manuscript Received April 7, 1997⊗

Downloaded via UNIV OF MASSACHUSETTS AMHERST on January 29, 2023 at 23:47:09 (UTC).
See https://pubs.acs.org/sharingguidelines for options on how to legitimately share published articles.

Monolayer and multilayer thin films consisting of anionic α-zirconium phosphate (α-ZrP) sheets and polycations (poly(allylamine hydrochloride) (PAH), cytochrome *c*) were characterized by transmission electron microscopy (TEM), ellipsometry, UV−visible absorbance spectroscopy, reflectance FT-IR, XPS, and X-ray diffraction. Titration and powder X-ray diffraction experiments confirm that exfoliation of α-ZrP begins to occur when enough tetra-(*n*-butylammonium) hydroxide (TBA^+OH^-) has been added to exceed single-layer packing of TBA^+ ions ($x \approx 0.50$) in the intercalation compound $Zr(HPO_4)_{2-x}(TBA^+PO_4^-)_x \cdot nH_2O$. The identical contrast of many sheets in TEM micrographs suggests that the suspension is unilamellar. Alternately dipping cationic substrates into α-ZrP-containing suspensions and aqueous PAH gives a multilayer film that resembles the corresponding bulk intercalation compound. X-ray photoelectron spectra of multilayer films show that they are Zr-rich, relative to α-ZrP, consistent with some corrosion during the exfoliation reaction. The α-ZrP/PAH layer pair thickness is 13/14.7 Å, as measured by ellipsometry/X-ray diffraction, respectively. A 13-layer pair film is sufficiently well-ordered in the stacking direction to give a Bragg peak in the diffraction pattern. The agreement between the bilayer thickness and the total film thickness, measured from Kiessig fringes in the low-angle part of the diffraction pattern, confirms that only a single dense α-ZrP or PAH monolayer is deposited in each adsorption step.

Introduction

Self-assembled thin films have been studied increasingly in recent years, because of both their fundamental interest as interfacial phases and their potential applications in a variety of surface-dependent technologies.[1] Thin films composed of alkanethiols, organosilanes, ceramic insulators, metals, and semiconductors are finding practical applications in the control of friction, adhesion, chemical sensing, microelectronics, and other areas.[2] While the self-assembly of organic monolayers on surfaces is now a well-understood process, the preparation of stable and ordered multilayer films remains a challenge, and relatively few approaches to it have been demonstrated. Most of these involve linking together sequentially grown self-assembling monolayers, through covalent,[3] ionic−covalent,[4] coordinate−covalent,[5] hydrogen-bonding,[6] or electrostatic interactions.[7−12]

† Current address: Department of Chemistry, University of Missouri, Columbia, MO 65211.

⊗ Abstract published in *Advance ACS Abstracts,* May 15, 1997.

(1) (a) Ulman, A. *An Introduction to Ultrathin Organic Films: From Langmuir-Blodgett to Self-Assembly*; Academic Press: Boston, 1991. (b) Fendler, J. H. *Chem. Mater.* **1996**, *8*, 1616. (c) Delamarche, E.; Michel, B.; Biebuyck, H. A.; Gerber, C. *Adv. Mater.* **1996**, *8*, 719.

(2) (a) Fendler, J. H. *Membrane Mimetic Approach to Advanced Materials*; Springer-Verlag: Berlin, 1992. (b) Bard, A. J. *Integrated Chemical Systems, a Chemical Approach to Nanotechnology*; Wiley: New York, 1994. (c) Kumar, A.; Abbott, N. L.; Kim, E.; Biebuyck, H. A.; Whitesides, G. M. *Acc. Chem. Res.* **1995**, *28*, 219.

(3) (a) Netzer, L.; Sagiv, J. *J. Am. Chem. Soc.* **1983**, *105*, 674. (b) Maoz, R.; Netzer, L.; Gun, J.; Sagiv, J. *J. Chim. Phys.* **1988**, *85*, 1059. (c) Tillman, A.; Ulman, A.; Penner, T. L. *Langmuir* **1989**, *5*, 101. (d) Nuzzo, R. G.; Allara, D. L. *J. Am. Chem. Soc.* **1983**, *105*, 4481. (e) Kakkar, A. K.; Yizchaik, S.; Roscoe, S. B.; Marks, T. J. *Thin Solid Films* **1994**, *242*, 142. (f) Ichinose, I.; Senzu, H., Kunitake, T. *Chem. Lett.* **1996**, 831.

(4) (a) Lee, H.; Kepley, L. J.; Hong, H.-G.; Mallouk, T. E. *J. Am. Chem. Soc.* **1988**, *110*, 618. (b) Lee, H.; Kepley, L. J.; Hong, H.-G.; Akhter, S.; Mallouk, T. E. *J. Phys. Chem.* **1988**, *92*, 2597. (c) Cao, G.; Hong, H.-G.; Mallouk, T. E. *Acc. Chem. Res.* **1992**, *25*, 420. (d) Akhter, S.; Lee, H.; Hong, H.-G.; Mallouk, T. E.; White, J. M. *J. Vac. Sci. Technol. A* **1989**, *7*, 1608. (e) Putvinski, T. M.; Schilling, M. L.; Katz, H. E.; Chidsey, C. E. D.; Mujsce, A. M.; Emerson, A. B. *Langmuir* **1990**, *6*, 1567. (f) Katz, H. E.; Schilling, M. L.; Chidsey, C. E. D.; Putvinski, T. M.; Hutton, R. S. *Chem. Mater.* **1991**, *3*, 699. (g) Evans, S. D.; Ulman, A.; Goppert-Berarducci, K. E.; Gerenser, L. J. *J. Am. Chem. Soc.* **1991**, *113*, 5866. (h) Umemura, Y.; Tanaka, K.-I.; Yamagishi, A. *J. Chem. Soc., Chem. Commun.* **1992**, 67. (i) Yang, H. C.; Aoki, K.; Hong, H.-G.; Sackett, D. D.; Arendt, M. F.; Yau, S.-L.; Bell, C. M.; Mallouk, T. E. *J. Am. Chem. Soc. 115*, 11855. (j) Frey, B. L.; Hanken, D. G.; Corn, R. M. *Langmuir* **1993**, *9*, 1815. (k) Byrd, H.; Pike, J. K.; Talham, D. R. *Chem. Mater.* **1993**, *5*, 709. (l) Byrd, H.; Whipps, S.; Pike, J. K.; Talham, D. R. *Thin Solid Films* **1994**, *244*, 768. (m) Zeppenfeld, A. C.; Fiddler, S. L.; Ham, W. K.; Klopfenstein, B. J.; Page, C. J. *J. Am. Chem. Soc.* **1994**, *116*, 9158. (n) O'Brien, J. T.; Zeppenfeld, G. L.; Richmond, G. L.; Page, C. J. *Langmuir* **1994**, *10*, 4657. (o) Byrd, H.; Snover, J. L.; Thompson, M. E. *Langmuir* **1995**, *11*, 4449. (p) Hanken, D. G.; Corn, R. M. *Anal. Chem.* **1995**, *67*, 3767. (q) Hoekstra, K. J.; Bein, T. *Chem. Mater.* **1996**, *8*, 1865.

S0897-4756(97)00027-6 CCC: $14.00 © 1997 American Chemical Society

Samsung Ex. 1031, Page 1 of 8
Samsung Electronics Co., Ltd., et al. v. Molecular Rebar Design, LLC
IPR2025-00355

For inorganic materials, self-assembly represents an interesting alternative to more traditional film-growth techniques, such as electroplating, electroless deposition, sol−gel processing, evaporation, sputtering, laser ablation, molecular beam epitaxy, and chemical vapor deposition. While each of these techniques is very useful for a range of materials and applications, all suffer to some extent from the loss of molecular connectivity that occurs during the deposition process. We reported recently the adaptation of the polyelectrolyte adsorption technique to sequential layering of structurally well-defined, colloidal inorganic polyanions with a variety of oligomeric and polymeric cations.[12] The advantage of this technique, which combines methods devised earlier by Iler[7a] and by Decher,[8] originates from the fact that the films incorporate semiinfinite, two-dimensional inorganic sheets. This feature effectively prevents the interpenetration of adjacent anion and cation layers, except at grain boundaries of the anion sheets, while maintaining the ease and generality of the polyelectrolyte adsorption process. The method can potentially be used to impart special mechanical, electronic, optical, and/or magnetic properties to the multilayer composites by choosing appropriate inorganic components, which so far include silicates,[11] transition-metal oxides and phosphates,[12] graphite oxide,[13] and lamellar chalcogenides.[14]

In this paper, we report a detailed study of the growth and characterization of prototypical multilayer films prepared from high charge density inorganic polyanions (α-zirconium phosphate) and organic polycations (poly(allylamine hydrochloride). The importance of the surface priming step is explored for different substrates, and time-resolved adsorption experiments give an idea of the kinetics of layer growth. Various surface-sensitive spectroscopies provide a probe of the film deposition process and the resulting structure, which can be compared with that of similarly grown but structurally very different polyelectrolyte thin films based on clays[11] or organic polyanions.[8]

Experimental Section

Materials. Poly(allylamine hydrochloride) (PAH, MW 50 000−65 000), 4-mercaptopyridine (4-MP), sodium 2-mercaptoacetate (MEA), and sodium 2-mercaptoethanesulfonate (MES) were used as received from Aldrich Chemical Co. (4-Aminobutyl)dimethylmethoxysilane (4-ABDMMS), from United Chemical Technologies, Inc., 2-mercaptoethylamine hydrochloride (2-MEA), and cytochrome *c* from Sigma Chemical Co. were used as received. All other chemicals were reagent grade and obtained from commercial sources.

Substrate Preparation. Polished (100) Si wafers were sonicated in CCl_4 for 15 min and then rinsed with 2-propanol and water. They were then sonicated in a hot piranha solution of H_2SO_4 and H_2O_2 (2:1) for 30 min. (**Caution**: this solution can react violently with organic compounds) and rinsed with copious amounts of water, then methanol, and finally 1:1 methanol/toluene before beginning the derivatization steps. The Si substrates, which were initially hydrophobic, became hydrophilic after this sequence of cleaning steps. Au substrates were prepared as described previously[4b] or were purchased from EMF Corp. (Ithaca, NY) as a 1000 Å Au film grown on a 50 Å Ti adhesion layer on 1 in. × 3 in. × 0.040 in. glass microscope slides. Quartz microscope slides (1 in. × 3 in × 1 mm) obtained from Chemglass, Inc., and mica substrates (0.5 in × 0.69 in. × 0.010 in.) from Spruce Pine Mica Co., were cleaned with a hot piranha solution of H_2SO_4 and H_2O_2 (2:1) for 30 min and rinsed with copious amounts of deionized water.

Preparation of α-$Zr(HPO_4)_2 \cdot H_2O$ (α-ZrP). Crystalline zirconium phosphate was prepared by the HF method as described by Alberti et al.,[15a] and its structure was confirmed by powder X-ray diffraction. Semicrystalline zirconium phosphate was prepared by the reflux method in 2.5 M H_3PO_4 for 48 h.[15b]

Exfoliation of α-$Zr(HPO_4)_2 \cdot H_2O$ Colloidal suspensions of α-ZrP were prepared by very slow dropwise titration with 0.5 M tetra-*n*-butylammonium hydroxide (TBA^+OH^-) to reach a constant pH of 8.0. Care was taken to avoid higher pH conditions, which can lead to substantial and rapid corrosion of the sheets, during the titration. Complete exfoliation of the solid takes more than 24 h and sometimes several days, depending on the size of the precursor crystals and pH of the titration reaction.[16a,b] The colloidal suspensions were prepared and stored at a relatively high concentration (25 mequiv/L), where they are turbid, and were adjusted before use to pH 8.0 with 0.1 M tetra-*n*-butylammonium hydroxide (TBA^+OH^-), followed by centrifugation to obtain uniform and stable translucent colloidal solution. The total amount of tetra-*n*-butylammonium hydroxide added was about equimolar with

(5) (a) Bell, C. M.; Keller, S. W.; Lynch, V. M.; Mallouk, T. E. *Mater. Chem. Phys.* **1993**, *35*, 225. (b) Bell, C. M.; Arendt, M. F.; Mallouk, T. E. *J. Am. Chem. Soc.* **1994**, *116*, 8374. (c) Ansell, M. A.; Zeppenfeld, A. C.; Yoshimoto, K.; Cogan, E. B.; Page, C. J. *Chem. Mater.* **1996**, *8*, 591.

(6) (a) Sun, L.; Kepley, L. J.; Crooks, R. M. *Langmuir* **1992**, *8*, 2101. (b) Arias, F.; Godinez, L. A.; Wilson, S. R.; Kaifer, A. E.; Echegoyen, L. *J. Am. Chem. Soc.* **1996**, *118*, 6086.

(7) (a) Iler, R. K. J. *Colloid Interface Sci.* **1966**, *21*, 569. (b) Ingersoll, D.; Kulesza, P. J.; Faulkner, L. R. *J. Electrochem. Soc.* **1994**, *141*, 140. (c) Mao, G.; Tsao, Y.; Tirrell, M.; Davis, H. T.; Hessel, V.; Ringsdorf, H. *Langmuir* **1993**, *9*, 3461. (d) Ferreira, M.; Cheung, J. H.; Rubner, M. F. *Thin Solid Films* **1994**, *244*, 806. (e) Cheung, J. H.; Fou, A. F.; Rubner, M. F. *Thin Solid Films* **1994**, *244*, 985. (f) Zhang, X.; Gao, M.; Kong, X.; Sun, Y.; Shen, J. *J. Chem. Soc., Chem. Commun.* **1994**, 1055. (g) Gao, M.; Kong, X.; Zhang, X.; Shen, J. *Thin Solid Films* **1994**, *244*, 815. (h) Sun, Y.; Zhang, X.; Sun, C.; Wang, Z.; Shen, J.; Wang, D.; Li, T. *Chem. Commun.* **1996**, 2379. (i) Moon, J. H.; Choi, J. U.; Kim, J. H.; Chung, H.; Hahn, J. H.; Kim, S. B.; Park, J. W. *J. Mater. Chem.* **1996**, *6*, 365.

(8) (a) Decher, G.; Hong, J.-D. *Makromol. Chem., Makromol. Symp.* **1991**, *46*, 321. (b) Decher, G.; Hong, J. D. *Ber. Bunsen-Ges. Phys. Chem.* **1991**, *95*, 1430. (c) Decher, G.; Hong, J.-D.; Schmitt, J. *Thin Solid Films* **1992**, *210/211*, 831. (d) Decher, G.; Schmitt, J. *Progr. Colloid Polym. Sci.* **1992**, *89*, 160. Decher, G.; Essler, F.; Hong, J.-D.; Lowack, K.; Schmitt, J.; Lvov, Y. *Polym. Prepr.* **1993**, *34*, 745. (e) Decher, G. *Nachr. Chem. Tech. Lab.* **1993**, *41*, 793. (f) Lvov, Y.; Decher, G.; Möhwald, H. *Langmuir* **1993**, *9*, 481. (g) Lvov, Y.; Decher, G.; Sukhorukov, G. *Macromolecules* **1993**, *26*, 5396. (h) Lvov, Y.; Hass, H.; Decher, G.; Möhwald, H.; Kalachev, A. *J. Phys. Chem.* **1993**, *97*, 12835. (i) Lvov, Y.; Essler, F.; Decher, G. *J. Phys. Chem.* **1993**, *97*, 13773. (j) Schmitt, J.; Grünewald, T.; Kjaer, K.; Pershan, P.; Decher, G.; Lösche, M. *Macromolecules* **1993**, *26*, 7058. (k) Decher, G.; Lvov, Y.; Schmitt, J. *Thin Solid Films* **1994**, *244*, 772.

(9) (a) Cooper, T. M.; Campbell, A. L.; Noffsinger, C.; Gunther-Greer, J.; Crane, R. L.; Adams, W. W. *MRS Symp. Proc.* **1994**, *351*, 239. (b) Cooper, T. M.; Campbell, A. L.; Crane, R. L. *Langmuir* **1995**, *11*, 2713.

(10) (a) Lvov, Y.; Hass, H.; Decher, G.; Möhwald, H. *Langmuir* **1994**, *10*, 4232. (b) Lvov, Y.; Ariga, K.; Kunitake, T. *Chem. Lett.* **1994**, 2323. (c) Lvov, Y.; Ariga, K.; Kunitake, T. *J. Am. Chem. Soc.* **1995**, *117*, 6117. (d) Ichinose, I.; Fujiyoshi, K.; Mizuki, S.; Lvov, Y.; Kunitake, T. *Chem. Lett.* **1996**, 257. (e) Isayama, M.; Nomiyama, K.; Kunitake, T. *Adv. Mater.* **1996**, *8*, 641.

(11) (a) Kleinfeld, E. R.; Ferguson, G. S. *Science* **1994**, *265*, 370. (b) Ferguson, G. S.; Kleinfeld, E. R. *Adv. Mater.* **1995**, *7*, 414.

(12) (a) Keller, S. W.; Kim, H.-N.; Mallouk, T. E. *J. Am. Chem. Soc.* **1994**, *116*, 8817. (b) Kaschak, D. M.; Mallouk, T. E. *J. Am. Chem. Soc.* **1996**, *118*, 4222.

(13) Kotov, N. A.; Dekany, I.; Fendler, J. H. *Adv. Mater.* **1996**, *8*, 637.

(14) Ollivier, P. J.; Mallouk, T. E., unpublished results.

(15) (a) Alberti, G.; Torracca, E. *J. Inorg. Nucl. Chem.* **1968**, *30*, 317. (b) Clearfield, A.; Stynes, J. A. *J. Inorg. Nucl. Chem.* **1964**, *26*, 117. (c) Clearfield, A.; Smith, D. *Inorg. Chem.* **1969**, *8*, 431. (d) Troup, J. M.; Clearfield, A. *Inorg. Chem.* **1977**, *16*, 3311.

(16) (a) Treacy, M. M. J.; Rice, S. B.; Jacobson, A. J.; Lewandowski, J. T. *Chem. Mater.* **1990**, *2*, 279. (b) Alberti, G.; Casciola, M.; Costantino, U. *J. Colloid Interface Sci.* **1985**, *107*, 256. (c) Alberti, G.; Marmottini, F. *J. Colloid Interface Sci.* **1993**, *157*, 513. (d) Alberti, G.; Casciola, M.; Costantino, U.; Vivani, R. *Adv.*

Samsung Ex. 1031, Page 2 of 8
Samsung Electronics Co., Ltd., et al. v. Molecular Rebar Design, LLC
IPR2025-00355

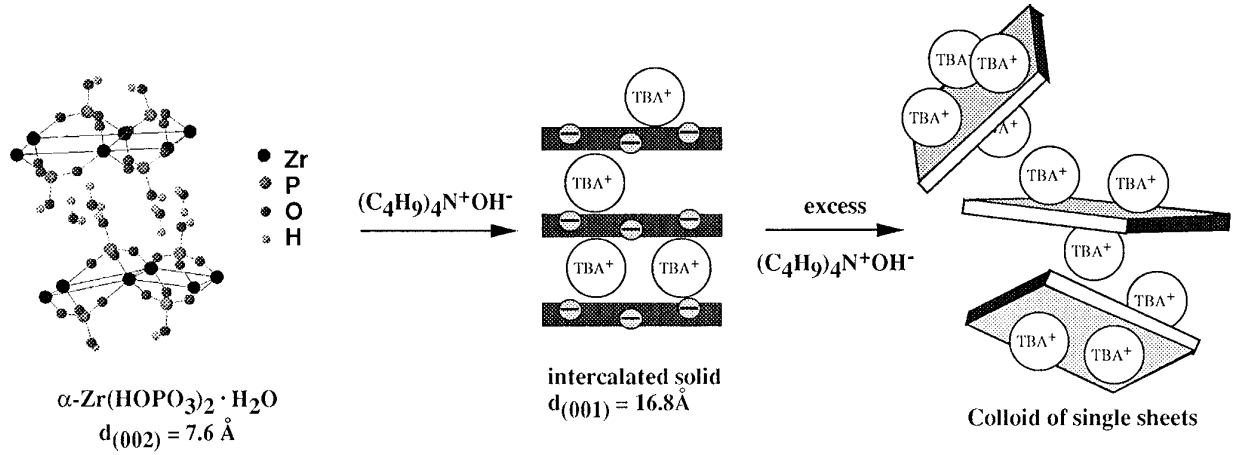

Figure 1. Process of exfoliation of layered α-$Zr(HPO_4)_2 \cdot H_2O$.

the amount of α-ZrP, giving an approximate composition of $Zr(HPO_4)(TBAPO_4) \cdot xH_2O$. The upper phase of centrifuged solution was diluted with deionized water to about 1 mequiv/L of α-ZrP prior to film deposition. The exact concentrations of colloidal α-ZrP were determined by ICP-AES analysis of the Zr content, after dissolving the colloid in 45% aqueous HF.

Preparation and Adsorption of Polyelectrolyte Solutions. Aqueous solutions of PAH (10 mM) and cytochrome *c* (0.1 mM) were adjusted to pH 7 using 0.1 M TBA^+OH^-. Layer deposition times were typically 15 min. Following each deposition step, the samples were washed with flowing deionized water, absolute ethanol, and deionized water again, and then dried with flowing Ar. The thickness change was routinely monitored by ellipsometry between adsorption steps.

Characterization of Substrates and Thin Films. Ellipsometric data were obtained using a Gaertner Model L2W26D ellipsometer with a HeNe laser (632.8 nm) light source. The incident angle was 70°, and the polarizer was set at 45°. Typically, the thicknesses of 5−7 spots/sample were measured and averaged. The substrate values that were used were measured values for Au substrates and the literature value (Ns = 3.875, Ks = −0.018) for Si substrates. The real part of the refractive index of the film was fixed at 1.54, which is a typical value for organic materials and which matched the measured values of films within about 0.1 during measurements. The imaginary part of the film refractive index was assumed to be zero.

Reflectance IR spectra were measured with a Nicolet 730 FT-IR spectrometer, which had Spectratech Inc. FT-80 film attachment that kept the angle of incidence fixed at 80°. The optical bench was purged with dry nitrogen gas, and the spectrometer was equipped with a liquid nitrogen cooled MCT-A detector. Spectra were recorded after 1024 scans at a resolution of 2 cm^{-1} and were referenced to spectra of the unmodified Au substrate. Samples for FT-IR measurements were prepared on 1 in. × 1 in. Au substrates. X-ray photoelectron spectra (XPS) were obtained using a Hewlett-Packard 5950A instrument with 256 multichannel resistor plates. All spectra were taken using the Al Kα line source at 1486.6 eV. The spectrometer has a typical resolution of 1.0 eV, with anode voltage and power settings of 15 kV and 800 W, respectively. The typical operating pressure was 5×10^{-9} Torr. Survey scans were performed at a takeoff angle of 52° to the surface normal. UV−visible spectra were collected on a Hewlett-Packard 8452A diode array spectrometer. Thin-film samples were measured on quartz substrates, using unmodified quartz as a reference.

Thin-film X-ray diffraction experiments were performed on a Siemens D-500 powder diffractometer, typically with multilayer films grown on single-crystal silicon substrates. X-ray powder diffraction patterns were obtained with a Philips X'Pert MPD powder diffractometer, using monochromatic Cu Kα radiation. Transmission electron microscopy (TEM) images were obtained with a JEOL 1200EXII microscope, at a 120 kV acceleration voltage and 80 μA filament current.

Results and Discussion

Exfoliation of α-Zirconium Phosphate. Figure 1 illustrates the intercalation and exfoliation of α-ZrP. The procedure is similar to that originally reported by Alberti and co-workers in their studies of alkylamine intercalation reactions, except that an ionic strong base is used instead of a neutral amine.[16] TBA^+ cations are forced to intercalate in the solid weak acid/aqueous strong base neutralization reaction, resulting in an intercalation compound with a 16.8 Å layer spacing and ultimately in a fully delaminated colloid.

Figure 2 shows cross sections of intercalated α-$Zr(HPO_4)_2 \cdot H_2O$, with the TBA^+ ions drawn to scale. In the hypothetical basal plane structure shown in Figure 2, there are two potentially ionizable phosphate groups on each side of the sheet for every TBA^+ ion (10 Å diameter). The cations are shown overlapping in projection, consistent with molecular models that allow interlocking of *n*-butyl groups. Since height of the interlayer gallery is 10.5 Å, the TBA^+ ions reside in a single-layer arrangement, and the stoichiometry is therefore $Zr(HPO_4)_{1.5}(TBA^+PO_4^-)_{0.5} \cdot xH_2O$. Experimentally, the observed stoichiometry of the single-layer intercalation compound is 0.38−0.50 TBA^+/Zr.[17] A double-layer arrangement with one TBA^+ cation per Zr, i.e., $Zr(HPO_4)_{1.0}(TBA^+PO_4^-)_{1.0} \cdot xH_2O$ would cover each sheet completely by TBA^+. However, this arrangement, which introduces cation−cation contacts between layers, is apparently unstable to exfoliation in water. When more TBA^+OH^- is added to $Zr(HPO_4)_{1.5}(TBA^+PO_4^-)_{0.5} \cdot xH_2O$, additional protons are ionized, and more TBA^+ ions bind to each side of the anionic sheets to give a colloidal suspension.

Powder X-ray diffraction patterns (Figure 3) show the progress of the exfoliation reaction. α-$Zr(HPO_4)_2 \cdot H_2O$ has a 7.6 Å layer spacing, and sharp *hkl* diffraction lines indicate that the layers are in registry. Intercalation produces the 16.8 Å phase, with apparent loss of in-plane registry, as evidenced by the disappearence of lines with $h, k \neq 0$. Interestingly, the restacked solid,

(17) Garcia, M. E.; Naffin, J. L.; Deng, N.; Mallouk, T. E. *Chem. Mater.* **1995**, *7*, 1968.

Samsung Ex. 1031, Page 3 of 8
Samsung Electronics Co., Ltd., et al. v. Molecular Rebar Design, LLC
IPR2025-00355

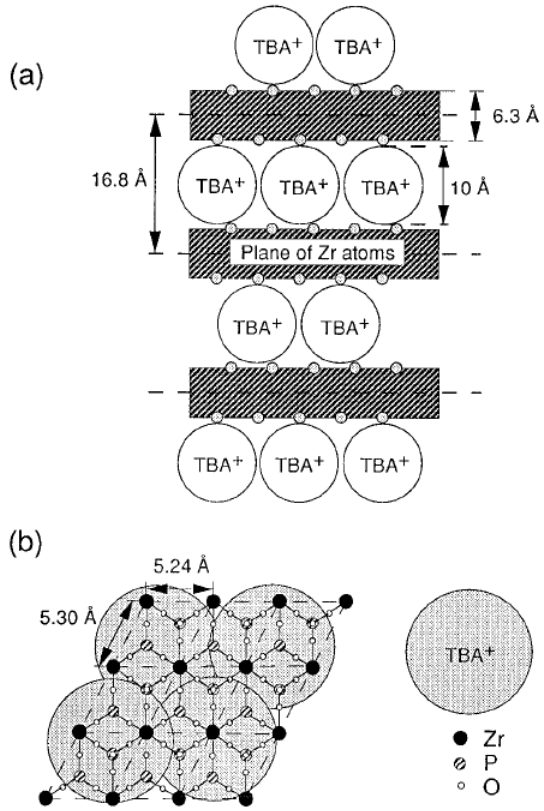

Figure 2. (a) Schematic drawing in cross section of TBA^+-intercalated α-ZrP and (b) stacking axis projection showing the packing density of TBA ions in $Zr(HPO_4)_{1.5}$-$(TBA^+PO_4^-)_{0.5}\cdot xH_2O$.

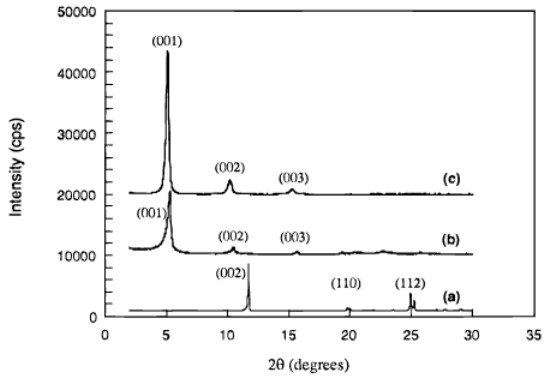

Figure 3. X-ray diffraction patterns of (a) α-ZrP, (b) $Zr(HPO_4)_{1-y}(TBA^+PO_4^-)_y\cdot xH_2O$ ($y = 0.50 \pm 0.04$), and (c) dried film of the restacked α-ZrP colloid on a flat Au substrate.

prepared as a thick film by drying the colloid on planar Si or Au substrates, also gives diffraction lines typical of an intercalation compound.[18] The restacked α-ZrP has a slightly larger interlayer spacing (17.3 Å) than the single-layer (fully loaded) intercalation compound, but the difference is slight, suggesting a single-layer arrangement of cations in the restacked phase as well. It should be recalled at this point that powder X-ray diffraction is sensitive primarily to the crystalline portion of the sample. The presence of a less well-ordered double-layer phase or of amorphous zirconium hydroxide in the restacked film would not be evident in this experiment.

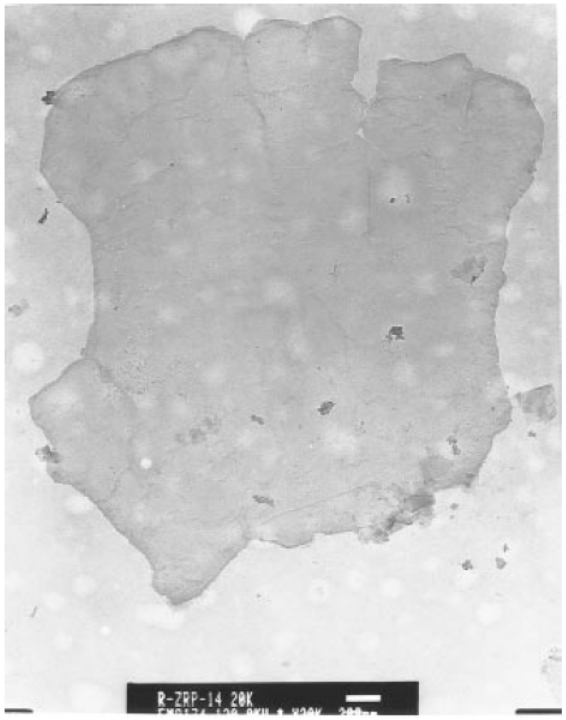

Figure 4. TEM micrograph of a single α-ZrP sheet, obtained by dipping a TEM grid into a 20 μM colloidal suspension at pH 8.0. Scale bar is 200 nm.

The morphology of the colloidal α-ZrP was also studied by TEM. Figure 4 shows a micrograph of a typical sheet, obtained by dipping a Formvar-coated Cu TEM grid in the colloidal suspension at low concentration. The sheet appears to be buckled slightly, possibly a consequence of differential substrate/sample shrinkage upon drying. The observation of many such sheets with identical TEM contrast and measured thicknesses of ca 1.0 nm by atomic force microscopy[19] support the hypothesis that these are unilamellar suspensions. The lateral dimensions of the two-dimensional α-ZrP sheets vary from about 0.1 to 5 μm, depending on the size and crystallinity of the precursor $\alpha\text{-}Zr(HPO_4)_2\cdot H_2O$ crystallites.

Adsorption of Substrate Priming Layers. The polyelectrolyte adsorption process often requires covalent anchoring of charged molecules to the substrate. Poor substrate priming typically results in patchy or dendritic multilayers, which ultimately form smoother films after many adsorption cycles.[20] Clean silicon, glass, quartz, and mica substrates were incubated in 1 wt % solutions of a silane-anchoring agent (4-ABDMMS) in anhydrous toluene for ca. 15 h, after which the previously hydrophilic substrates became hydrophobic. Ellipsometry of the anchored Si substrates showed that

(18) Sasaki, T.; Watanabe, M.; Hashizume, H.; Yamada, H.; Nakazawa, H. *Chem. Commun.* **1996**, 229.

(19) Kaschak, D. M.; Johnson, S. A.; Kim, H.-N.; Mallouk, T. E., manuscript in preparation.

(20) Kleinfeld, E. R.; Ferguson, G. S. *Chem. M*

Samsung Ex. 1031, Page 4 of 8
Samsung Electronics Co., Ltd., et al. v. Molecular Rebar Design, LLC
IPR2025-00355

Table 1. Surface Properties of Different Anchoring Agents on Silicon, Gold, Quartz, Glass, and Mica Substrates[a]

substrate	surface treatment	exposed functional group	surface polarity
Si(100)	H_2O_2/H_2SO_4(1:3)	$SiO_2 \cdot nH_2O$	hydrophilic
Si(100)	4-ABDMMS	$-NH_2$	hydrophobic
Au(111)	CH_3CH_2OH	Au(111)	hydrophobic
Au(111)	H_2O_2/H_2SO_4(1:3)	$AuO_x \cdot nH_2O$	hydrophilic
Au(111)	2-MEA	$-NH_3^+$	hydrophilic
Au(111)	4-mercaptopyridine	$-C_5H_4NH^+$	hydrophilic
Au(111)	MA	$-CO_2^-$	hydrophilic
Au(111)	MES	$-SO_3^-$	hydrophilic
$AuO_x \cdot nH_2O$	4-ABDMMS	$-NH_2$	hydrophobic
Mica	toluene	anionic silicate	hydrophilic
Mica	H_2O_2/H_2SO_4 (1:3)	anionic silicate	hydrophilic
Mica	4-ABDMMS	$-NH_2$	hydrophobic
glass/quartz	CH_3CH_2OH	$SiO_2 \cdot nH_2O$, anionic glass	hydrophilic
glass/quartz	H_2O_2/H_2SO_4(1:3)	$SiO_2 \cdot nH_2O$, anionic glass	hydrophilic
glass/quartz	4-ABDMMS	$-NH_2$	hydrophobic

[a] 4-ABDMMS: (4-aminobutyl)dimethylmethoxysilane. 2-MEA: 2-mercaptoethylamine, hydrochloric acid salt. MA: mercaptoacetic acid, sodium salt. MES: mercaptoethanesulfonic acid, sodium salt.

they were very uniformly modified over the surface of the sample and that the surface coating had a thickness of 22 ± 2 Å. This value corresponds well to the combined thickness of the anchoring molecule (ca. 7 Å) and the native SiO_2 layer (15 ± 2 Å) on the Si (111) surface.[21] Gold substrates, which were derivatized with 0.010 M 2-MEA in absolute ethanol for 24 h, became hydrophilic, whereas 4-ABDMMS-modified Au substrates, which had been previously oxidized in piranha solution, became hydrophobic. Au substrates were also modified with 0.0010 M 4-MP, 0.0050 M MA, and 0.0050 M MES in absolute ethanol, to examine the effect of the charge of the anchoring layer on film growth. All three of these mercaptans, like 2-MEA, produced a hydrophilic Au surface, consistent with binding of the thiolate group to the surface.

Table 1 summarizes the cleaning and priming of various substrates and indicates the hydrophobic or hydrophilic nature of the resulting surface. In all cases this character is consistent with covalent binding of the anchoring molecule to the substrate.

Adsorption of Colloidal Zirconium Phosphate Monolayers on Cationic Surfaces. Figure 5 shows schematically how the sequential adsorption of polyelectrolyte monolayers proceeds. The substrate is first derivatized with a cation-forming molecule, for example, (4-aminobutyl)dimethylmethoxysilane. The aliphatic amine groups are protonated at neutral pH and electrostatically bind polyanions, which are adsorbed in this case from a colloidal suspension. The negatively charged colloid monolayer overcompensates the positive charge of the alkylammonium groups, leaving a negatively charged surface and inhibiting further colloid deposition. Subsequent adsorption of a cationic polyelectrolyte again inverts the surface charge, and the process (steps 2 and 3 in Figure 5) can be repeated to build up the desired number of layers.

Figure 5b shows the ellipsometric thickness increase with deposition time for the first α-ZrP layer on 2-MEA/Au. Although very similar layer thicknesses were observed with 4-ABDMMS/Si, the first α-ZrP layer is adsorbed faster on 4-ABDMMS/Si (about 7 min to formation of a 10 Å monolayer) than on 2-MEA/Au. The reason for this difference is not clear. It is possible that the metallic substrate, because of image charges that compensate the charge of the primer layer, presents a

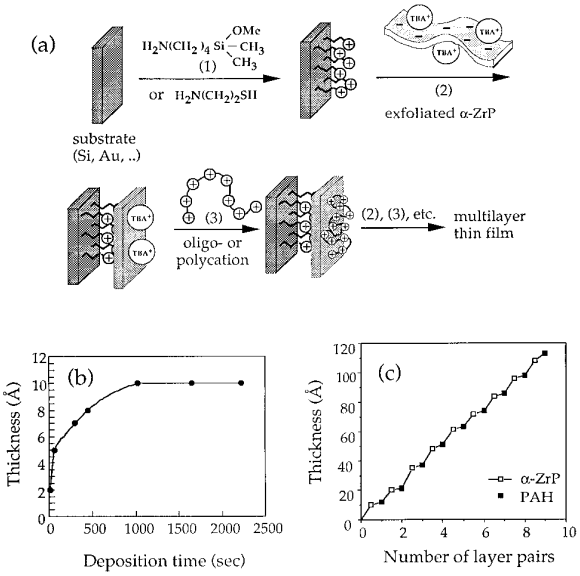

Figure 5. (a) Reaction scheme for sequential adsorption of α-ZrP polyanions and organic oligo- or polycations. (b) Thickness change vs time for adsorption of a-ZrP from a 0.1 mequiv/L colloidal solution onto 2-MEA/Au. (c) Ellipsometric thickness data for alternate adsorption of α-ZrP and PAH on 2-MEA/Au. Each adsorption step was 15 min. Layer thicknesses were calculated using a film refractive index of 1.54.

surface that has less electrostatic attraction for the colloid. Both substrates have the same apparent affinity for cationic polyelectrolytes after the first layer of α-ZrP is grown, and the multilayer film-growth process is substrate-independent after the first layer. Table 2 compares ellipsometric thicknesses of the first α-ZrP layer and the first PAH layer adsorbed directly on various surfaces. The pK_a values given in Table 2 are those of the monomeric compounds, and polyelectrolyte effects will decrease the surface pK_a (the pH at which the monolayer is 50% protonated) of charged acids (4-ABDMMS, 2-MEA, and 4-MP) and increase that of neutral acids (MA and 2-MES) used as anchoring layers. Nevertheless, it is clear from these data that α-ZrP monolayers grow on positively charged, amine-terminated surfaces at neutral pH, whereas PAH monolayers grow on negatively charged surfaces. Neither polyelectrolyte produces a complete monolayer on the pyridine-terminated 4-MP/Au surface, consistent with its low charge density at neutral pH.

(21) Haller, I. *J. Am. Chem. Soc.* **1978**, *100*, 8050.

Samsung Ex. 1031, Page 5 of 8
Samsung Electronics Co., Ltd., et al. v. Molecular Rebar Design, LLC
IPR2025-00355

Table 2. Effect of Anchoring Agents on Binding the First Polyelectrolyte Layer[d]

substrate	anchoring agent	pK_a	surface charge (+/−) at pH 7	thickness of first α-ZrP layer (Å)	thickness of first PAH layer (Å)
Si	4-ABDMMS	10.77[a]	positive	12 ± 1	0
AuO_2/Au	4-ABDMMS	10.77[a]	positive	10 ± 1	0
Au	2-MEA	10.75[b]	positive	11 ± 1	0
Au	4-MP	5.37[b]	neutral	0	2 ± 1
Au	MA	3.58[b]	negative	0	5 ± 1
Au	2-MES	0.70[c]	negative	0	5 ± 1

[a] pK_a of *n*-butylamine. [b] Values are obtained from: *Ionisation Constants of Organic Acids in Aqueous Solution*; Serjeant, E. P., Dempsey, B.; Pergamon Press: Oxford, U.K., 1979. [c] pK_a of benzenesulfonic acid. [d] 4-ABDMMS: (4-aminobutyl)dimethylmethoxysilane. 4-MP: 4-mercaptopyridine. MA: mercaptoacetic acid, sodium salt. MES: mercaptoethanesulfonic acid, sodium salt. 2-MEA: 2-mercaptoethylamine, hydrochloric acid salt.

Layer-by-Layer Growth of Multilayer Films. The stepwise growth of multilayer films can be conveniently monitored by ellipsometry. Figure 5c shows a plot of film thickness vs number of layer pairs for multilayer films consisting of PAH polycations and anionic α-ZrP sheets. When α-ZrP is alternately adsorbed with PAH, the anion−cation bilayer thickness is 13 Å, consistent with the approximate dimensions of 7.6 Å α-ZrP lamellae[15c] and 5 Å monolayers of uncoiled PAH.[8] The average thickness increase in the deposition of the first α-ZrP layer (Table 2) is 11 ± 1 Å, which is about 3.5 Å thicker than expected for a 7.6 Å sheet. The additional thickness can be assigned to the loosely bound TBA^+ ions, which charge-compensate the anionic α-ZrP surface. Adsorption of PAH onto the α-ZrP surface is reflected in an apparent thickness increase of only 2 Å, despite the fact that a PAH monolayer on Au/MA or Au/2-MES has a thickness of 5 ± 1 Å. The difference may again be ascribed to the displacement of surface-bound TBA^+.

As in other polyelectrolyte deposition strategies,[7−13] each adsorption step is self-limiting because of repulsion of like-charged polyelectrolytes. For example, anionic polyelectrolytes such as poly(acrylic acid) do not grow on α-ZrP, and cationic polyelectrolytes such as PAH do not bind to positively charged surfaces such as 2-MEA/Au or 4-ABDMMS/Si. As with other polyelectrolytes, these adsorption reactions are fast. Kleinfeld and Ferguson have reported that hectorite/poly(diallylamine) layers are complete in 5 s,[11] and Lvov et al. showed that each of their polycation or polyanion layers are completely formed within 15 min.[10] In the present system, even with relatively long adsorption times, ellipsometric measurements do not indicate adsorption of bilayers and structural reorganization in the inorganic adsorption step, as was found for hectorite/poly(diallylamine). It should be noted that the latter colloids have lower charge density and are grown from more concentrated solutions,[11] and these parameters may be important determinants of film structure.

X-ray reflectometry provides a good check of ellipsometric film thicknesses. From the positions of Kiessig fringes in the low-angle part of the diffraction pattern, the total film thickness may be calculated, independent of the refractive index. Also, Bragg diffraction peaks, found at higher angle, contain information about the internal structure and degree of order of the film along the stacking axis. Figure 6 shows the X-ray diffraction pattern of a 13-bilayer film of α-ZrP/PAH grown on Si/4-ABDMMS. From the Kiessig fringes (inset), the total thickness of the film was calculated to be 174 Å, in reasonably good agreement with the ellipsometrically derived thickness of 160 Å. The difference reflects an overestimation, on the order of 10%, of the film refractive index. The appearance of a Bragg peak in the vicinity of 6° 2θ confirms that α-ZrP and PAH layers are not arranged randomly in the film but stack as an intercalation compound. The position of the Bragg peak gives a bilayer spacing of 14.7 Å, again slightly larger than the ellipsometric average of 13.0 Å, the discrepancy again arising from the error in refractive index.

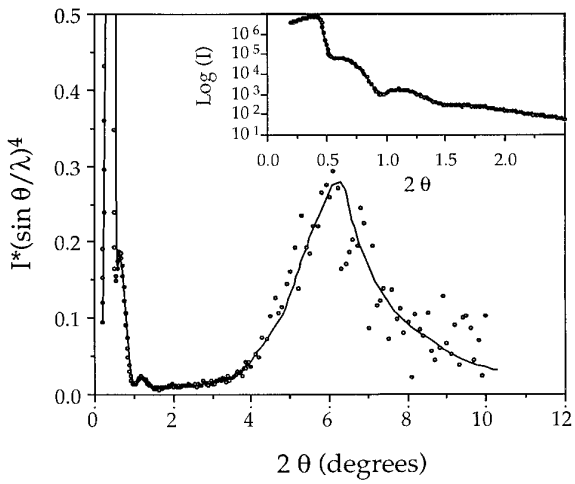

Figure 6. Thin-film X-ray diffraction pattern of 13 α-ZrP/PAH layer pairs on Si. Inset shows low-angle data (Kiessig fringes) plotted on a logarithmic scale.

The agreement of the total thickness of the film and the Bragg spacing, i.e., the fact that their ratio is 11.8 for a 13-layer film, provides compelling evidence that the film grows in monolayers, rather than in bilayers or some other disordered stacking arrangement. The slightly lower than expected refractive index is reasonable when one considers that randomly sized and shaped α-ZrP sheets cannot tile the surface with unit efficiency. The diffraction results are consistent with parallel studies in which energy-transfer reactions between fluorophore-labeled PAH layers were used as a "spectroscopic ruler" to measure layer interpenetration. The data in that study also showed that the formation of a PAH or α-ZrP layer is an irreversible process and that little or no interlayer mixing occurs in subsequent adsorption cycles.[12b]

Spectroscopic Characterization of α-ZrP/Polycation Films. Multilayer films on gold were further characterized by reflection−absorption FT-IR spectroscopy. Figure 7 shows infrared spectra of multilayer films of α-ZrP/PAH and of bulk α-ZrP/PAH, prepared by combining colloidal α-ZrP with an aqueous solution of PAH. The infrared mode assignments for both the film and bulk α-ZrP/PAH samples are ε

Samsung Ex. 1031, Page 6 of 8
Samsung Electronics Co., Ltd., et al. v. Molecular Rebar Design, LLC
IPR2025-00355

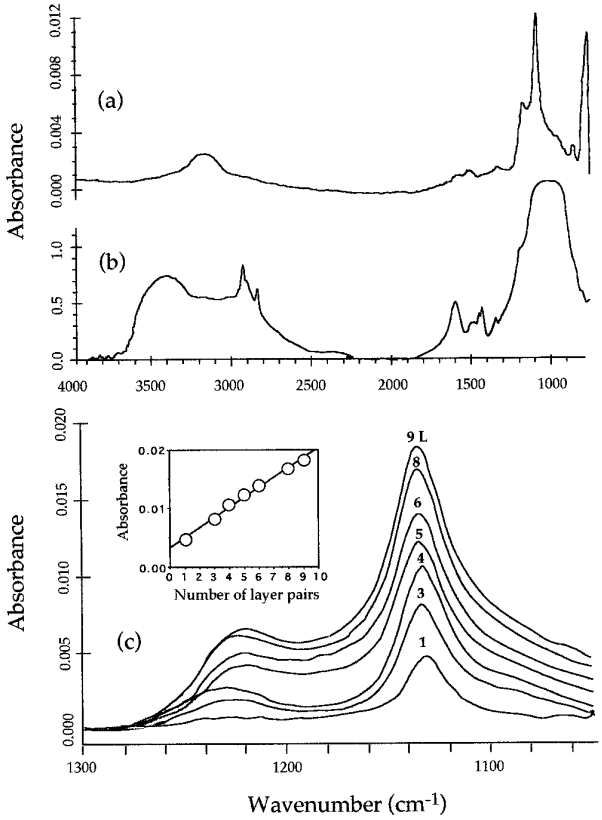

Figure 7. (a) Reflection−absorption IR spectrum of six α-ZrP/PAH layer pairs on 2-MEA/Au. (b) Transmission IR spectrum of bulk α-ZrP/PAH with KBr. (c) Reflection−absorption spectra of α-ZrP/PAH multilayers in the P−O stretching region. Inset: plot of P−O absorbance at 1140 cm^{-1} vs numbers of α-ZrP/PAH layer pairs.

Table 3. Infrared Spectral Assignments for α-ZrP/PAH

mode	bulk	film	ref
O−H (H_2O) stretching	3440		23a
N−H stretching	3240	3200	23a
O−H (H_2O) stretching	3050		23a
νas (C−H)	2963		23a
νs (C−H)	2876		23a
(p)−O−H stretching	2380		23a
(p)−O−H stretching	2060		23a
O−H (H_2O) def bending	1630	1630	23a
N−H def bending	1521	1545	23a
CH_2 bending	1471	1460	23a
CH_2 bending	1382	1370	23a
H_2O def bending	1255		23a
ν_{as} (PO_4)	1120	1220	4i
ν_s (PO_4)	1040	1130	4i
	960	1010	4i
	840	906	4i

The typical (P)−O−H deformation mode of orthophosphoric acid is in the range 1600−1740 cm^{-1}, which is much higher than that of bulk α-$Zr(HPO_4)_2 \cdot H_2O$, 1310 cm^{-1}.[22] These peaks are present in the spectrum of both the bulk and thin-film intercalation compounds, consistent with only partial ionization of the layers. Symmetric and asymmetric C−H stretching vibrations, at 2962 and 2876 cm^{-1}, and a broad OH stretching vibration attributed to hydrogen-bonded water, centered at 3400 cm^{-1}, are also evident in the bulk spectrum but are too weak to be observed distinctly in the spectrum of the thin film. Interestingly, N−H stretching of intercalated PAH is evident in the multilayer film spectrum, even though C−H stretching modes of the polymer are too weak to be observed. This suggests that the C−H bonds lie predominantly parallel to the gold substrate.[3d] The bulk spectrum also shows stronger water stretching and deformation bands, relative to N−H stretching, than does the thin film. This may indicate a higher degree of hydration in the more poorly ordered bulk intercalation compound.

(22) (a) Socrates, G. In *Infrared Characteristic Group Frequencies*, 2nd ed.; John Wiley & Sons: New York, 1992; Chapter 9, p 74 and Chapter 17, p 177. (b) Corbridge, D. E. C.; Lowe, E. J. *J. Chem. Soc.* **1954**, 4555. (c) Vliers, D. P.; Schoonheydt, R. A. *J. Chem. Soc., Faraday Trans. 1* **1985**, *81*, 2009.

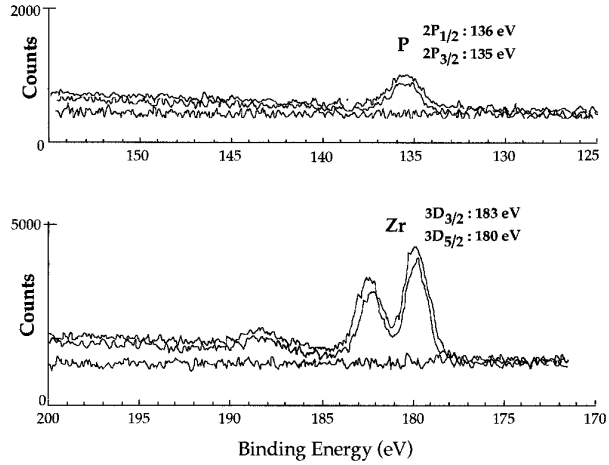

Figure 8. XPS spectra of 1, 7, and 9 α-ZrP/PAH layer pairs on 2-MEA/Au, showing peaks for (a) P (135/136 eV) and (b) Zr (180/183 eV).

The strongest absorbances in both the bulk and thin film spectra arise from symmetric and asymmetric P−O stretching modes of the phosphate groups. Figure 7c shows the linear increase in absorbance in the P−O stretching region, at 1130 cm^{-1}, with number of α-ZrP layers grown on Au, confirming the regularity of the film growth process. The P−O stretching peaks of the thin films are sharp and appear at significantly higher frequency than those of bulk α-ZrP/PAH, 1040 and 1120 cm^{-1}. Curious features of these spectra are the nonzero intercept of the layer growth plot, which may reflect a change in extinction coefficient of the $\nu_s(PO_4)$ band, a shift to higher frequency of the $\nu_s(PO_4)$ band, and a shift to lower frequency of the $\nu_{as}(PO_4)$ band, as more layers are applied. At present we have no definitive explanation for these observations. We note however that the degree of protonation of the polyamine, and therefore its interaction with the α-ZrP lamellae, could be different in the monolayer, multilayer, and bulk cases. From the O−H and N−H stretching regions of the IR spectra, it is also apparent that the bulk solid is more hydrated than the thin film.

X-ray photoelectron spectroscopy (XPS) provides a measure of film composition that complements the infrared analysis. A particularly important issue is the Zr:P ratio in the films, which will be larger than 1:2 if substantial corrosion (to produce insoluble ZrO_2 and soluble phosphate) occurs in either the exfoliation or deposition steps. Figure 8 shows XPS spectra, for both a single α-ZrP layer and for α-ZrP/PAH multilayer films on Au substrates. The $3d_{3/2}$ zirconium peak at 183 eV is observable for a single layer of

Samsung Ex. 1031, Page 7 of 8
Samsung Electronics Co., Ltd., et al. v. Molecular Rebar Design, LLC
IPR2025-00355

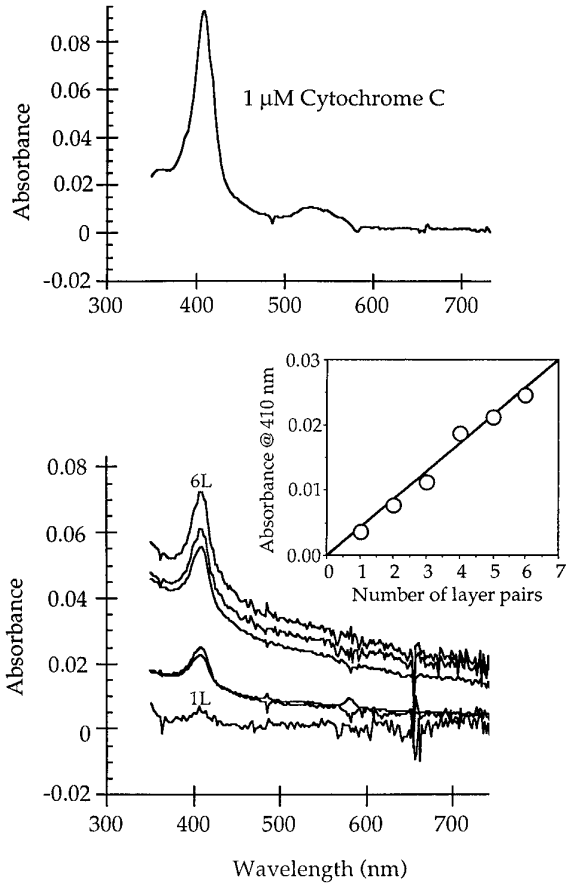

Figure 9. UV−visible spectra of (a) 1 μM cytochrome *c* (cyt *c*) in H_2O and (b) α-ZrP/cyt *c* thin films on quartz. Inset: plot of the cyt *c* Soret band absorbance at 410 nm (baseline corrected) vs number of α-ZrP/cyt *c* layer pairs.

phosphorus 2p peak at 135 eV is not easily resolved from the noise, because of its lower XPS sensitivity. For the α-ZrP/PAH multilayer films, both peaks are clearly seen, and a zirconium-to-phosphorus atomic ratio of 1:(1.6 ± 0.2) can be calculated from peak areas and a lamellar structural model.[4i] This calculation uses inelastic mean free paths of 15 Å for photoelectrons emitted from both Zr and P. The calculated Zr:P ratio is quite insensitive to variation of the mean free path, as long as the same value is used for both elements. This result indicates that some corrosion of the sheets does in fact occur in the exfoliation/adsorption process.

The incorporation of cationic proteins into polyelectrolyte thin films[10b,c] and bulk intercalation compounds[23] is now well documented. In bulk compounds there is evidence that the tertiary structure, spectroscopic, and redox properties of heme proteins are retained upon intercalation.[24] The alternate adsorption of α-ZrP monolayers with the positively charged protein cytochrome *c* (cyt *c*) was monitored by UV−visible spectroscopy, using optically transparent quartz substrates. The linear growth with layer number of the cyt *c* Soret band absorbance at 410 nm is shown in Figure 9. The average absorbance change per α-ZrP/cyt c layer pair (on each side of the quartz) is 0.0022 ± 0.0002, and the measured extinction coefficient, from a solution of 1.0 μM cyt c in water, is 9.31×10^7 mol^{-1} cm^2. From these data, and the density (1.3 g/cm^3)[25] and molecular weight (12 384 g/mol) of cyt *c*, the average thickness of an individual cyt *c* layer can be calculated as 23 ± 2 Å, assuming that the layers have the same packing density as bulk cyt *c*. This value is consistent with the width of the protein, which is a globule of 25 × 25 × 37 Å dimensions in the crystalline state.[25] It is also in good agreement with the 32 Å layer spacing reported for the bulk intercalation compound,[24] allowing 8 Å for the thickness of the α-ZrP sheet. The bulk layer spacing is slightly greater than the average film thickness measured by ellipsometry, 26 ± 3 Å. The discrepancy between the optical absorbance/powder XRD and ellipsometric data may arise from an overestimation of the refractive index (1.54 ± 0*i*) of α-ZrP/cyt *c* multilayer films.

Conclusions

The structure of a prototypical inorganic self-assembled multilayer, α-ZrP/PAH, has been studied by ellipsometry, TEM, reflection−absorption infrared spectroscopy, XPS, and X-ray diffraction. Although there are subtle differences, the picture that emerges from this study is a multilayer film that is essentially a bulk analogue of an intercalation compound. The α-ZrP lamellae tile cationic surfaces densely and stack with PAH to produce a multilayer film that has sufficient crystallographic order in the stacking direction to give a broad Bragg diffraction peak. The adsorption reactions of both the lamellar polyanion and the polycation are self-limiting, and film thicknesses determined by X-ray diffraction and ellipsometry are consistent with the irreversible adsorption of a single monolayer in each step.

The advantage of this method, compared to other techniques for growing inorganic thin films, is that it is experimentally very simple, so that complex multilayer sequences can be grown quickly and easily with control of structure at the monolayer level. The method can be applied equally well to large-area substrates or to small, nonplanar ones. These properties make the technique amenable to the preparation of a number of interesting aperiodic structures for electron and energy transfer reactions.[26,27] Among the most important fundamental questions remaining to be addressed are the kinetics and mechanism of the tiling process, the detailed lateral structure of the films, and the specific chemistry of the edges of the colloidal sheets. These issues are now being investigated by scanning probe microscopy and other techniques and will be discussed in a future publication.

Acknowledgment. We thank Drs. Rosemary Walsh and Wayne Kaboord for assistance with TEM experiments. This work was supported by a grant from the National Science Foundation (CHE-9396243).

CM970027Q

(23) Ding, Y.; Jones, D. J.; Torres, P. M.; Roziere, J. *Chem. Mater.* **1995**, *7*, 562.
(24) Kumar, C. V.; McLendon, G. L. *Chem. Mater.* **1997**, *9*, 863.
(25) Takano, T.; Kallai, O. B.; Swanson, R.; Dickerson, R. E. *J. Biol. Chem.* **1973**, *248*, 5244.
(26) Keller, S. W.; Johnson, S. A.; Yonemoto, E. H.; Brigham, E. S.; Mallouk, T. E. *J. Am. Chem. Soc.* **1995**, *117*, 12879.
(27) Feldheim, D. L.; Grabar, K. C.; Natan, M. J.; Mallouk, M. E. *J. Am. Chem. Soc.* **1996**, *118*, 7640.

Samsung Ex. 1031, Page 8 of 8
Samsung Electronics Co., Ltd., et al. v. Molecular Rebar Design, LLC
IPR2025-00355